Scientific article doi: 10.1590/2175-3369.013.e20200345

A long-term monthly assessment of land surface temperature and normalized difference vegetation index using Landsat data

Uma avaliação mensal de longo prazo da temperatura da superfície da terra e índice de vegetação de diferença normalizada usando dados Landsat

Subhanil Guha[a]

[a] National Institute of Technology Raipur, Department of Applied Geology, Raipur, India

How to cite: Guha, S. (2021). A long-term monthly assessment of land surface temperature and normalized difference vegetation index using Landsat data. *urbe. Revista Brasileira de Gestão Urbana*, v.13, e20200345. https://doi.org/10.1590/2175-3369.013.e20200345

Abstract

The present study assesses the monthly variation of land surface temperature (LST) and the relationship between LST and normalized difference vegetation index (NDVI) in Raipur City of India using one hundred and eighteen Landsat images from 1988 to 2019. The results show that a monthly variation is observed in the mean LST. The highest mean LST is found in April (38.79°C), followed by May (36.64°C), June (34.56°C), and March (32.11°C).The lowest mean LST is observed in January (23.01°C), followed by December (23.76°C), and November (25.83°C). A moderate range of mean LST is noticed in September (27.18°C), October (27.22°C), and February (27.88°C). Pearson's linear correlation method is used to correlate LST with NDVI. The LST-NDVI correlation is strong negative in October (-0.62), September (-0.55), and April (-0.51). The moderate negative correlation is developed in March (-0.40), May (-0.44), June (-0.47), and November (-0.39). A weak negative correlation is observed in December (-0.21), January (-0.24), and February (-0.29). The change in weather elements and variation in land surface characteristics contribute to the monthly fluctuation of mean LST and LST-NDVI correlation. The study will be an effective one for the town and country planners for their future estimation of land conversion.

Keywords: Landsat. Land surface. Land surface temperature. Normalized difference vegetation index. Raipur.

SG is Researcher, Ph.D. in Applied Geology, e-mail: subhanilguha@gmail.com

Resumo

O presente estudo avalia a variação mensal da temperatura da superfície terrestre (LST) e a relação entre lST e o índice de vegetação de diferença normalizado (NDVI) na cidade de Raipur, na Índia, utilizando cento e dezoito imagens landsat de 1988 a 2019. Os resultados mostram que uma variação mensal é observada no LST médio. O LST médio mais elevado é encontrado em abril (38,79oC), seguido por maio (36.64oC), junho (34.56oC) e março (32.11oC). O LST médio mais baixo é observado em janeiro (23.01oC), seguido por dezembro (23.76oC) e novembro (25,83oC). Uma gama moderada de LST médio é notada em setembro (27.18oC), outubro (27.22oC) e fevereiro (27.88oC). O método linear de correlação de Pearson é usado para correlacionar LST com NDVI. A correlação LST-NDVI é fortemente negativa em outubro (-0,62), setembro (-0,55) e abril (-0,51). A correlação negativa moderada é desenvolvida em março (-0,40), maio (-0,44), junho (-0,47) e novembro (-0,39). Uma correlação negativa fraca é observada em dezembro (-0,21), janeiro (-0,24) e fevereiro (-0,29). A alteração dos elementos meteorológicos e a variação das características da superfície terrestre contribuem para a flutuação mensal da correlação média LST e LST-NDVI. O estudo será eficaz para os planeadores da cidade e do país para a sua futura estimativa da conversão de terras.

Palavras-chave: *Landsat. Superfície de terra. Temperatura da superfície do terreno. Índice de vegetação de diferença normalizado. O Raipur.*

Introduction

The thermal infrared (TIR) region of the electromagnetic spectrum has a huge potential in determining the nature and characteristics of land surface dynamics in any natural environment along with the visible and near-infrared (VNIR) and shortwave infrared (SWIR) regions (Chen et al., 2006; Ghobadi et al., 2014; Guha et al., 2018; Guha & Govil, 2020; Guha & Govil, 2021a; Guha & Govil, 2019; Alexander, 2020). Land surface temperature (LST) is a major factor to assess the biogeochemical actions in the formation of land surface materials and it is the most essential parameter to evaluate the ecological condition of rural or urban areas (Tomlinson et al., 2011; Hao et al., 2016). LST varies with the changes of tone, texture, pattern, and association of the land surface types in any region (Hou et al., 2010). Generally, green vegetation and water bodies present low LST, whereas a built-up area, bare rock surface, or dry soil reflects high LST (Guha et al., 2019). Thus, LST-related studies are very important in urban and land use planning and development (Li et al., 2017; Guha, Govil & Besoya, 2020; Guha, Govil, Gill & Dey, 2020a). Urban heat islands and urban hot spots are very common term in an urban environment and are indicated by the zone of very high LST inside the urban bodies (Guha et al., 2017). The most popular spectral index is the normalized difference vegetation index (NDVI) which is used in extracting green vegetation (Yuan et al., 2017; Guha & Govil, 2021b; Mondal et al., 2011; Guha, 2016; Guha, Govil, Gill & Dey, 2020b; Guha, Govil, Dey et al., 2020; Guha, Govil, Gill & Dey, 2020c; Guha, Govil & Diwan, 2020). NDVI is directly used in the determination of land surface emissivity and thus is a significant factor for LST estimation (Sobrino et al., 2004; Carlson & Ripley, 1997).

Currently, the relationship between LST and NDVI was constructed using thermal infrared remote sensing technology and only some satellite sensors have the thermal bands like Landsat, MODIS, and ASTER (Wen et al., 2017; Guha et al., 2017). The required wavelength of these thermal bands is 8-14 μm for LST determination. An infrared thermometer instrument is used to validate the derived LST values (Li et al., 2017; Guha, Govil & Besoya, 2020; Guha, Govil, Gill & Dey, 2020a; Guha et al., 2017). LST-NDVI relationship was applied in most of the thermal remote sensing studies that were conducted with temporal discrete data sets on the urban environment, e.g., Tokyo, Melbourne, Shiraz, Raipur (Shigeto, 1994; Jamei et al., 2019; Fatemi & Narangifard, 2019; Guha & Govil, 2021c). Ferelli et al. (2018) correlate LST with NDVI in Monte Hermosoof Argentina. Fewer studies are available on the long-term and continuous seasonal correlation among LST, NDVI, and LULC in a tropical city.

A reverse relationship is built between LST and the concentration of green vegetation and thus, NDVIis used as an important factor for determining LST in most of the LST retrieval methods (Voogt & Oke, 2003; Gutman & Ignatov, 1998; Goward et al., 2002; Govil et al., 2019; Guha, 2021; Govil et al., 2020).

There are so many valuable research articles found on LST-NDVI relationships that were conducted mainly in the Chinese landscape (Gui et al., 2019; Qu et al., 2020; Qu et al., 2018; Cui, Wang, Qu, Singh, Lai, Jiang& Yao, 2019; Cui, Wang, Qu, Singh, Lai& Yao, 2019; Yao, Cao et al., 2019; Yao, Wang, Gui et al., 2017; Yao, Wang, Huang, Chen et al., 2018; Yao, Wang et al., 2019; Yao, Wang, Huang et al., 2017; Yao, Wang, Huang, Zhang et al., 2018; Yuan et al., 2020). Some recent studies successfully analyze the LST-NDVI correlation in some tropical Indian cities (Kikon et al., 2016; Kumar & Shekhar, 2015; Mathew et al., 2018; Mathew et al., 2017; Sannigrahi et al., 2018; Singh et al., 2017). The nature of LST and NDVI varies due to the seasonal change of evaporation, precipitation, moisture content, air temperature, etc. But, time-series analysis of the monthly variation in the LST-NDVI relationship in a tropical Indian city is rare.

It is a necessary task to build a month-wise LST-NDVI correlation for the sustainable development of town and country planning. Thus, to determine the characteristic features of monthly variation of LST-NDVI correlation, Raipur City of India was selected as it is not under any kind of extreme climatic condition and it is a smart city with a rapid land conversion. Generally, the LST-NDVI correlation is negative on the tropical cities of similar environmental conditions of Raipur. But, the strength of the LST-NDVI relationship can change temporally, seasonally, and spatially. The relationship is changed with time as the land surface materials change with time. Elevation and slope are two main physiographic influencing factors that generate a negative correlation with LST. Wind speed and humidity are two climatic factors that create a negative relationship with LST. The relationship also depends on the LULC types as vegetation, soil, water, or built-up area change the values of NDVI as well as LST. Different seasons also play a significant role in the LST-NDVI relationship as the growth of vegetation and increase of LST primarily depend on seasonal change. But, no specific conclusion can draw between LST and NDVI by using a small number of remotely sensed data or within a short duration of research. A strong conclusion on the LST-NDVI relationship can be drawn only after the analyses of the multi-temporal and multi-seasonal data sets for a long-term continuous timeframe. Thus, large Landsat data sets are necessary to obtain a reliable result on this relationship. The present study analyzes the nature, strength, and trend of the effect of LST on NDVI and the LST-NDVI correlation on different types of LULC and their seasonal variation from 1988 to 2019. Thus, the new direction of the study is the long-term monthly change of LST-NDVI correlation analysis using the time-series data of Landsat sensors. The objective of the current research is to analyze the response of mean LST and LST-NDVI correlation in different months.

Study area and data

Figure 1 shows the research place (Raipur City of India) of the present research work. Figure 1(a) presents the outline map of India where Chhattisgarh State is located in the middle part (Source: Survey of India). Figure 1(b) presents the outline map of Chhattisgarh State with districts (Source: Survey of India). Figure 1(c) represents the false colour composite (FCC) image of Raipur City from recent Landsat 8 data (Date: 7 November 2018) where blue, green, and red bands of the image are filtered by the green, red, and infrared bands, respectively. False colour composite images are the combination of bands other than visible red, green, and blue as the red, green, and blue components of the display. These images are useful to allow us to distinguish various types of land surface materials that are difficult to identify by the naked eye or true colour composite image. Figure 1(d) indicates the contour map (Date: 11 October 2011) of the city from Advanced Spaceborne Thermal Emission and Reflection Radiometer (ASTER) Digital Elevation Model (DEM) data (Source: USGS). The city extends from 21°11'22"N to 21°20'02"N and from 81°32'20"E to 81°41'50"E. The total area of the city is approximately 164.23 km^2. The only big river in the area is Mahanadi. The south of the city is covered by dense forests. Geologically the city is very stable and no such major geological hazards are seen in the area. The central part of the city has a higher elevation compared to the periphery area. According to India Meteorological Department (IMD), Raipur is under the savannah type of climate. Table 1 presents the climatic data of Raipur from 1981-2012 (Source: IMD). May is the hottest month followed by April, June, and March. July is the rainiest month followed by August, June, and September. October and November are the post-monsoon months that experience pleasant weather conditions. December (the coldest month), January, and February are the winter months. The pre-monsoon and winter months (including November) remain dry compared to the monsoon and post-monsoon months.

Table 1 –Climate data for Raipur City (1981–2012)

Weather Elements	January	February	March	April	May	June	July	August	September	October	November	December
Maximum Temp (°C)	31.5	34.8	39.8	43.2	45.2	44.4	36.1	33.7	34.4	37.7	32.5	30.8
Minimum Temp (°C)	8.6	11.3	15.7	19.7	22.2	21.6	21.2	21.7	21.3	16.8	11.6	8.9
Mean Temp (°C)	20.7	23.4	28.9	32.3	34.7	31.7	27.8	27.2	27.8	27.6	23.1	20.3
Mean Monthly Rainfall (mm)	13.7	13.4	11.9	8.9	30.3	221.1	326.9	299.9	200.5	50.4	9.8	6.6
Average Relative Humidity (%)	47	35	28	22	27	52	76	79	73	59	51	49

Source: IMD (2020).

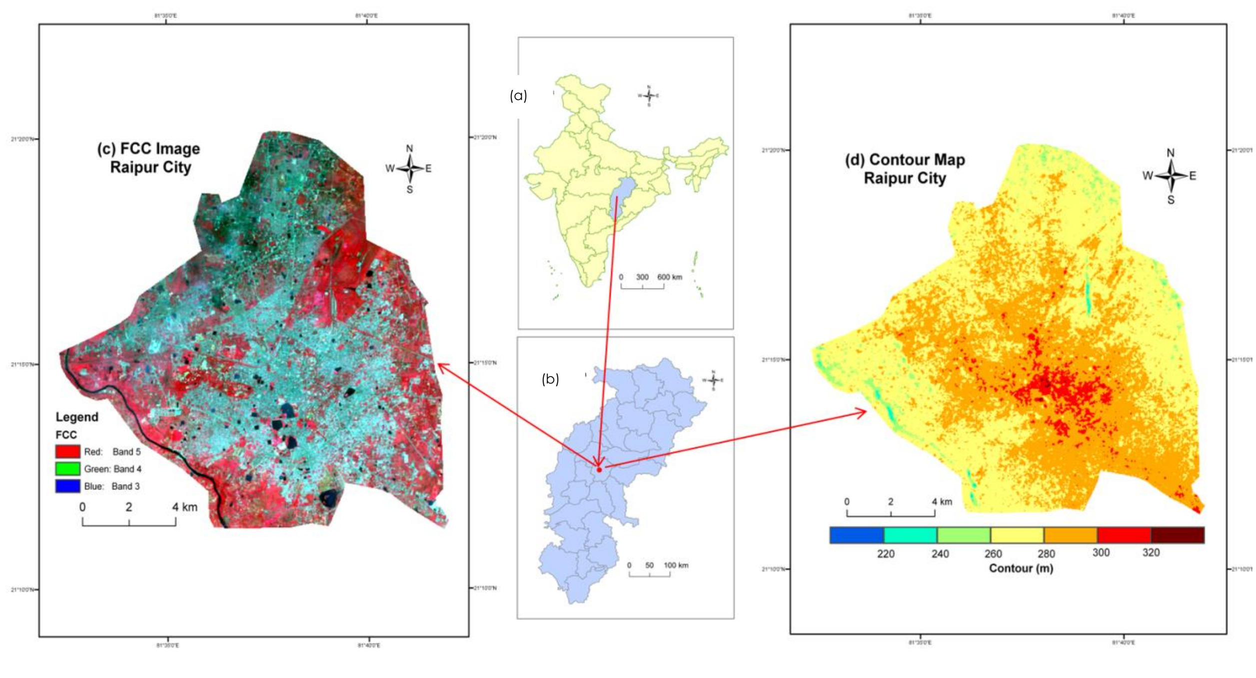

Figure 1 – Location of the study area (a) India (b) Chhattisgarh (c) FCC image of Raipur (d) Contour Map of Raipur showing the contours of 220 m, 240 m, 260 m, 280 m, 300 m, and 320 m. Source: Authors (2020).

Table 2 shows the resolution and wavelength information visible to near-infrared (VNIR) bands, shortwave infrared (SWIR) bands, and thermal infrared (TIR) bands of different types of Landsat satellite sensors.

Table 2 – Band and wavelength information about various types of Landsat sensors

Landsat 5 TM			Landsat 7 ETM+			Landsat 8 OLI/TIRS		
Bands	**Wavelength (μm)**	**Resolution (m)**	**Bands**	**Wavelength (μm)**	**Resolution (m)**	**Bands**	**Wavelength (μm)**	**Resolution (m)**
Band1-Blue	0.45-0.52	30	Band1-Blue	0.45-0.52	30	Band1-Ultra Blue	0.435-0.451	30
Band2-Green	0.52-0.60	30	Band2-Green	0.52-0.60	30	Band2-Blue	0.452-0.512	30
Band3-Red	0.63-0.69	30	Band3-Red	0.63-0.69	30	Band3-Green	0.533-0.590	30
Band4-NIR	0.76-0.90	30	Band4-NIR	0.77-0.90	30	Band4-Red	0.636-0.673	30
Band5-SWIR1	1.55-1.75	30	Band5-SWIR1	1.55-1.75	30	Band5-NIR	0.851-0.879	30
Band6-TIR	10.40-12.50	120*(30)	Band6-TIR	10.40-12.50	60**(30)	Band6-SWIR1	1.566-1.651	30
Band7-SWIR2	2.08-2.35	30	Band7-SWIR2	2.09-2.35	30	Band7-SWIR2	2.107-2.294	30
			Band8-Pan	0.52-0.90	15	Band8-Pan	0.503-0.676	15
						Band9-Cirrus	1.363-1.384	30
						Band10-TIR1	10.60-11.19	100***(30)
						Band11-TIR2	11.50-12.51	100***(30)

Note:*TM band 6 was acquired at 120 m resolution, but products are resampled by USGS to 30 m pixels.**ETM+ band 6 is acquired at 60 m resolution, but products are resampled by USGS to 30 m pixels.***TIRS bands 10 and 11are acquired at 100 m resolution, but products are resampled by USGS to 30 m pixels. Source: USGS.

One hundred and eighteen available cloud-free Landsat TM, ETM+, and OLI/TIRS data from 1988 to 2019 were freely downloaded from the USGS Data Centre (Table 2) to conduct the whole study. OLI/TIRS dataset has two TIR bands (bands 10 and 11). This large dataset was prepared by taking eleven data from January, fifteen from February, thirteen from March, ten from April, seventeen from May, four from June, four from September, thirteen from October, fifteen from November, and sixteen from December. There are very few cloud-free data sets available in the wet season (June-September), and this phenomenon could have an impact on the result of the retrieved LST. These Landsat data sets passed over the Raipur City every day between 10:00 AM to 10:30 AM. Hence, there is a scope to retrieve the LST of the study area at a specific time every day. The TIR band 10 data (100 m resolution) was applied for the current research due to better-calibrated certainty (Guha et al., 2018). The TIR band 10 data was resampled to 30 m x 30 m pixel size by the USGS data centre. TM data has only one TIR band (band 6) of 120 m resolution that was also resampled to 30 m x 30 m pixel size by the USGS data centre. ETM+ data has a TIR band (band 6) of 60 m resolution, and it was again resampled to 30 m x 30 m pixel size by the USGS data centre. The spatial resolution of the VNIR bands of the three types of Landsat sensors is 30 m.

Table 3 – Specification of TM, ETM+, and OLI/TIRS data used in the present study

Landsat scene ID	Date of acquisition	Time (UTC)	Path/Row	Sun elevation (°)	Sun azimuth (°)	Cloud cover (%)	Earth-Sun distance (astronomical unit)	Resolution of VNIR bands (m)	Resolution of TIR bands (m)
LT51420451988021BKT00	21-Jan-88	04:25:17	142/044	36.59	139.02	0.00	0.98	30	120
LT51420451990010BKT02	10-Jan-90	04:18:43	142/044	34.63	139.85	0.00	0.98	30	120
LT51420451992016ISP00	16-Jan-92	04:20:22	142/044	35.26	139.03	3.00	0.98	30	120
LT51420451993018ISP00	18-Jan-93	04:17:47	142/044	35.14	137.86	0.00	0.98	30	120
LT51420451996027ISP00	27-Jan-96	04:00:14	142/044	33.31	132.27	0.00	0.98	30	120
LT51420452005019BKT00	19-Jan-05	04:42:17	142/044	38.92	143.21	0.00	0.98	30	120
LT51420452007025BKT00	25-Jan-06	04:51:03	142/044	40.86	143.96	0.00	0.98	30	120
LT51420452009014BKT01	14-Jan-09	04:41:09	142/044	38.24	144.11	0.00	0.98	30	120
LT51420452011020BKT00	20-Jan-11	04:46:03	142/044	39.52	144.02	0.00	0.98	30	120
LC81420452015015LGN01	15-Jan-15	04:56:09	142/044	40.22	147.71	0.01	0.98	30	100
LC81420452018023LGN00	23-Jan-18	04:56:05	142/044	41.34	145.80	0.14	0.98	30	100
LT51420451989055BKT00	24-Feb-89	04:25:59	142/044	43.93	128.98	0.00	0.98	30	120
LT51420451990042BKT00	11-Feb-90	04:17:45	142/044	39.09	131.39	0.00	0.98	30	120
LT51420451991045ISP00	14-Feb-91	04:16:55	142/044	39.64	130.41	0.00	0.98	30	120
LT51420451992048ISP00	17-Feb-92	04:20:15	142/044	40.89	130.26	4.00	0.98	30	120
LT51420451993050BKT00	19-Feb-93	04:18:04	142/044	41.21	128.89	0.00	0.98	30	120
LE71420452002051BKT00	20-Feb-02	04:44:56	142/044	46.09	135.11	0.00	0.98	30	60
LT51420452004049BKT00	18-Feb-04	04:35:03	142/044	43.76	133.39	0.00	0.98	30	120
LT51420452006054BKT00	23-Feb-06	04:46:49	142/044	47.31	134.66	0.00	0.98	30	120
LT51420452009046KHC01	15-Feb-09	04:41:59	142/044	44.35	135.85	0.00	0.98	30	120
LT51420452010049KHC00	18-Feb-10	04:47:02	142/044	45.89	136.27	7.00	0.98	30	120
LC81420452015047LGN01	16-Feb-15	04:55:55	142/044	46.67	139.41	0.01	0.98	30	100
LC81420452016050LGN01	19-Feb-16	04:56:00	142/044	47.48	138.61	0.10	0.98	30	100
LC81420452017052LGN00	21-Feb-17	04:56:01	142/044	48.28	137.76	0.00	0.98	30	100
LC81420452018055LGN00	24-Feb-18	04:55:51	142/044	49.09	136.84	0.07	0.98	30	100
LC81420452019042LGN00	11-Feb-19	04:55:52	142/044	45.33	140.84	0.00	0.98	30	100
LT51420451989071BKT00	12-Mar-89	04:25:33	142/044	48.55	123.00	0.00	0.99	30	120
LT51420451990074BKT02	15-Mar-90	04:16:41	142/044	47.52	119.81	0.00	0.99	30	120
LT51420451991077ISP00	18-Mar-91	04:17:34	142/044	48.58	118.92	0.00	0.99	30	120
LT51420451992080ISP00	20-Mar-91	04:20:18	142/044	49.87	118.28	0.00	0.99	30	120
LE71420452003070SGS01	11-Mar-03	04:44:52	142/044	51.76	128.43	4.00	0.99	30	60
LT51420452004081BKT00	21-Mar-04	04:35:14	142/044	53.26	121.40	0.00	0.99	30	120
LT51420452007073BKT00	14-Mar-07	04:51:04	142/044	53.78	128.95	2.00	0.99	30	120
LT51420452009078KHC00	19-Mar-09	04:42:44	142/044	54.10	124.40	2.00	0.99	30	120
LC81420452014076LGN01	17-Mar-14	04:56:36	142/044	55.95	129.38	0.00	0.99	30	100
LC81420452015079LGN01	20-Mar-15	04:55:41	142/044	56.69	127.93	0.02	0.99	30	100
LC81420452016082LGN01	22-Mar-16	04:55:53	142/044	57.61	126.77	0.00	0.99	30	100
LC81420452017084LGN00	25-Mar-17	04:55:44	142/044	58.46	125.46	0.00	0.99	30	100
LC81420452018071LGN00	12-Mar-18	04:55:43	142/044	54.19	131.16	2.10	0.99	30	100
LT51420451992112BKT00	21-Apr-92	04:20:02	142/044	57.53	102.14	0.00	1.00	30	120
LT51420451995104ISP01	14-Apr-95	04:05:06	142/044	52.75	103.75	0.00	1.00	30	120
LE71420452001112SGS00	22-Apr-01	04:46:12	142/044	63.60	106.77	0.00	1.00	30	60
LE71420452002115SGS01	25-Apr-02	04:44:53	142/044	63.79	104.70	0.00	1.00	30	60
LE71420452003102BKT00	12-Apr-03	04:44:52	142/044	61.11	112.94	0.00	1.00	30	60
LT51420452004113BKT00	22-Apr-04	04:36:01	142/044	61.43	104.47	1.00	1.00	30	120
LT51420452009110BKT00	20-Apr-09	04:43:24	142/044	62.67	107.39	0.00	1.00	30	120
LT51420452010113KHC00	23-Apr-10	04:46:58	142/044	63.95	106.44	0.00	1.00	30	120
LC81420452016114LGN01	23-Apr-16	04:55:38	142/044	65.99	108.18	0.00	1.00	30	100
LC81420452017084LGN00	10-Apr-17	04:55:44	142/044	58.46	125.46	0.00	0.99	30	100
LT51420451991141ISP00	21-May-91	04:18:39	142/044	59.92	87.09	1.00	1.01	30	120
LE71420452002131SGS00	11-May-02	04:44:54	142/044	65.61	94.50	5.00	1.00	30	60
LT51420452004145BKT00	24-May-04	04:36:54	142/044	64.25	86.72	0.00	1.00	30	120
LT51420452005131BKT00	11-May-05	04:43:22	142/044	65.34	94.16	0.00	1.00	30	120
LT51420452006134BKT00	14-May-06	04:48:12	142/044	66.63	93.11	6.00	1.01	30	120
LT51420452007137BKT00	17-May-07	04:50:37	142/044	67.20	91.75	0.00	1.01	30	120
LT51420452008140BKT01	19-May-08	04:44:32	142/044	65.93	89.64	0.00	1.01	30	120
LT51420452009142KHC00	22-May-09	04:44:00	142/044	65.88	88.22	1.00	1.00	30	120
LT51420452010145BKT01	25-May-10	04:46:51	142/044	66.53	87.12	0.00	1.00	30	120
LT51420452011132KHC00	12-May-11	04:45:42	142/044	65.90	94.11	0.00	1.00	30	120
LC81420452013137LGN02	13-May-13	04:58:06	142/044	69.04	92.30	2.54	1.01	30	100
LC81420452014140LGN01	20-May-14	04:55:38	142/044	68.56	90.40	5.46	1.01	30	100
LC81420452015143LGN01	23-May-15	04:55:10	142/044	68.48	88.84	9.84	1.01	30	100
LC81420452016146LGN01	25-May-16	04:55:44	142/044	68.61	87.48	0.26	1.01	30	100
LC81420452017132LGN00	12-May-17	04:55:30	142/044	68.25	95.17	0.28	1.01	30	100
LC81420452018135LGN00	15-May-18	04:55:08	142/044	68.27	93.32	0.30	1.01	30	100
LC81420452019138LGN00	18-May-19	04:55:43	142/044	68.51	91.70	0.00	1.01	30	100
LT51420452005163BKT00	12-Jun-05	04:43:39	142/044	65.27	81.43	0.00	1.00	30	120
LT51420452006166BKT00	15-Jun-06	04:48:42	142/044	66.32	81.13	4.00	1.01	30	120
LT51420452009174KHC00	23-Jun-09	04:44:35	142/044	64.96	80.76	0.00	1.00	30	120
LC81420452018167LGN00	16-Jun-18	04:55:01	142/044	67.74	81.10	2.31	1.01	30	100
LT51420451996267ISP00	23-Sep-96	04:14:16	142/044	51.81	120.64	2.00	1.00	30	120
LT51420452001264SGI00	21-Sep-01	04:36:11	142/044	56.36	125.04	1.00	1.00	30	120
LE71420452002259SGS00	16-Sep-02	04:43:55	142/044	58.78	123.87	1.00	1.00	30	60
LC81420452014268LGN01	25-Sep-14	04:56:11	142/044	59.21	134.18	0.81	1.00	30	100
LT51420451988293BKT00	19-Oct-88	04:26:40	142/044	48.50	137.09	4.00	0.99	30	120
LT51420451991285BKT02	12-Oct-91	04:20:12	142/044	42.22	131.85	6.00	0.99	30	120
LT51420451992288BKT00	14-Oct-92	04:17:37	142/044	48.16	132.43	0.00	0.99	30	120
LT51420451996299ISP00	25-Oct-96	04:15:55	142/044	45.37	136.48	5.00	0.99	30	120
LE71420452001288SGS00	15-Oct-01	04:44:20	142/044	52.23	140.69	6.00	0.99	30	60
LT51420452001296SGI00	23-Oct-01	04:35:57	142/044	48.90	141.22	0.00	0.99	30	120
LT51420452004289BKT00	15-Oct-04	04:40:36	142/044	51.63	139.65	4.00	0.99	30	120
LT51420452006294BKT01	21-Oct-06	04:50:19	142/044	51.50	144.97	0.00	0.99	30	120
LT51420452009286KHC00	13-Oct-09	04:46:12	142/044	53.04	140.48	0.00	0.99	30	120
LT51420452011292KHC00	19-Oct-11	04:44:07	142/044	51.29	142.15	1.00	0.99	30	120
LC81420452015287LGN01	14-Oct-15	04:56:07	142/044	54.32	144.18	0.99	0.99	30	100
LC81420452016290LGN01	16-Oct-16	04:56:27	142/044	53.58	145.43	0.00	0.99	30	100
LC81420452018295LGN00	22-Oct-18	04:55:59	142/044	51.96	147.33	0.02	0.99	30	100
LT51420451988325BKT01	20-Nov-88	04:26:43	142/044	40.65	145.10	0.00	0.98	30	120
LT51420451989327BKT00	23-Nov-89	04:20:05	142/044	39.18	143.73	0.00	0.98	30	120
LT51420451991317ISP00	13-Nov-91	04:20:19	142/044	41.53	142.35	1.00	0.99	30	120
LT51420451993322ISP00	18-Nov-93	04:18:01	142/044	39.98	142.68	1.00	0.98	30	120
LT51420451996315ISP00	10-Nov-96	04:16:41	142/044	41.61	141.11	7.00	0.99	30	120
LE71420451999315SGS00	11-Nov-99	04:49:00	142/044	45.72	149.96	0.00	0.99	30	60
LT51420452004321BKT00	16-Nov-04	04:41:11	142/044	43.41	148.58	0.00	0.98	30	120
LT51420452005323BKT01	19-Nov-05	04:44:37	142/044	43.18	149.85	2.00	0.98	30	120
LT51420452006326BKT01	22-Nov-06	04:50:37	142/044	43.19	151.69	0.00	0.98	30	120
LT51420452008316BKT00	11-Nov-08	04:39:17	142/044	44.41	147.38	1.00	0.98	30	120
LC81420452013329LGN01	25-Nov-13	04:57:43	142/044	43.28	153.97	0.00	0.98	30	100
LC81420452014316LGN01	12-Nov-14	04:56:21	142/044	46.22	152.46	7.59	0.98	30	100
LC81420452016322LGN01	17-Nov-16	04:56:27	142/044	44.87	153.13	0.00	0.98	30	100
LC81420452017324LGN01	20-Nov-17	04:56:20	142/044	44.22	153.32	1.75	0.98	30	100
LC81420452019314LGN00	10-Nov-19	04:56:29	142/044	46.82	152.20	0.64	0.99	30	100
LT51420451988357BKT00	22-Dec-88	04:26:25	142/044	35.86	144.63	1.00	0.98	30	120
LT51420451992352ISP00	17-Dec-92	04:17:26	142/044	35.02	143.08	0.00	0.98	30	120
LT51420451994357ISP00	23-Dec-94	04:09:30	142/044	33.44	140.84	0.00	0.98	30	120
LT51420451995344BKT00	10-Dec-95	03:56:47	142/044	33.01	139.15	0.00	0.98	30	120
LE71420452000350SGS00	15-Dec-00	04:46:31	142/044	38.94	150.22	0.00	0.98	30	60
LE71420452002355SGS00	21-Dec-02	04:44:25	142/044	38.23	149.09	0.00	0.98	30	60
LT51420452004353BKT00	18-Dec-04	04:41:52	142/044	38.12	148.74	0.00	0.98	30	120
LT51420452006358BKT00	24-Dec-06	04:50:51	142/044	38.79	150.28	2.00	0.98	30	120
LT51420452008348KHC01	13-Dec-08	04:40:17	142/044	38.45	148.87	1.00	0.98	30	120
LT51420452009350KHC00	16-Dec-09	04:46:44	142/044	38.90	150.21	1.00	0.99	30	120
LT51420452010353BKT00	19-Dec-10	04:45:59	142/044	38.59	149.75	0.00	0.98	30	120
LC81420452013345LGN01	11-Dec-13	04:57:42	142/044	40.63	153.52	0.00	0.98	30	100
LC81420452016354LGN02	19-Dec-16	04:56:22	142/044	39.71	152.38	0.01	0.98	30	100
LC81420452017356LGN00	22-Dec-17	04:56:19	142/044	39.53	152.00	0.07	0.98	30	100
LC81420452018359LGN00	25-Dec-18	04:55:59	142/044	39.40	151.57	0.01	0.98	30	100
LC81420452019346LGN00	12-Dec-19	04:56:25	142/044	40.45	153.18	0.19	0.98	30	100

Source: Author (2020).

Methodology

Retrieving LST from Landsat data

In this study, the mono-window algorithm was applied to retrieve LST from multi-temporal Landsat satellite sensors where three necessary parameters are ground emissivity, atmospheric transmittance, and effective mean atmospheric temperature (Qin et al., 2001; Wang et al., 2016; Wang et al., 2019; Sekertekin & Bonafoni, 2020). At first, the original TIR bands (100 m resolution for Landsat 8 OLI/TIRS data, 60 m resolution for Landsat 7 ETM+ data, and 120 m resolution for Landsat 5 TM data) were resampled into 30 m by the USGS data centre for further application.

The TIR pixel values are firstly converted into radiance from digital number (DN) values. Radiance for TIR band of Landsat 5 TM data and Landsat 7 ETM+ data is obtained using Eq. (1) (USGS):

$$L_{\lambda} = \left[\frac{L_{MAX\,\lambda} - L_{MIN\,\lambda}}{QCAL_{MAX} - QCAL_{MIN}} \right] * \left[Q_{CAL} - QCAL_{MIN} \right] + L_{MIN\,\lambda} \qquad (1)$$

where, L_{λ} is Top of Atmosphere (TOA) spectral radiance (Wm^{-2}sr^{-1}mm^{-1}), Q_{CAL} is the quantized calibrated pixel value in DN, $L_{MIN\,\lambda}$ (Wm^{-2}sr^{-1}mm^{-1}) is the spectral radiance scaled to $QCAL_{MIN}$, $L_{MAX\,\lambda}$ (Wm^{-2}sr^{-1}mm^{-1}) is the spectral radiance scaled to $QCAL_{MAX}$, $QCAL_{MIN}$ is the minimum quantized calibrated pixel value in DN and $QCAL_{MAX}$ is the maximum quantized calibrated pixel value in DN. $L_{MIN\,\lambda}$, $L_{MAX\,\lambda}$, $QCAL_{MIN}$, and $QCAL_{MAX}$ values are obtained from the metadata file of Landsat TM and ETM+ data. Radiance for Landsat 8 TIR band is obtained from Eq. (2) (Zanter, 2019):

$$L_{\lambda} = M_L . Q_{CAL} + A_L \qquad (2)$$

where, L_{λ} is the TOA spectral radiance (Wm^{-2}sr^{-1}mm^{-1}), M_L is the band-specific multiplicative rescaling factor from the metadata, A_L is the band-specific additive rescaling factor from the metadata, Q_{CAL} is the quantized and calibrated standard product pixel values (DN). All of these variables can be retrieved from the metadata file of Landsat 8 OLI/TIRS data.

For Landsat 5 TM data and Landsat 7 ETM+ data, the reflectance value is obtained from radiances using Eq. (3) (USGS):

$$\rho_{\lambda} = \frac{\pi . L_{\lambda} . d^2}{ESUN_{\lambda} . \cos\theta_s} \qquad (3)$$

where, ρ_{λ} is unitless planetary reflectance, L_{λ} is the TOA spectral radiance (Wm^{-2}sr^{-1}µm^{-1}), d is Earth-Sun distance in astronomical units, $ESUN_{\lambda}$ is the mean solar exo-atmospheric spectral irradiances (Wm^{-2}µm^{-1}) and θ_s is the solar zenith angle in degrees. $ESUN_{\lambda}$ values for each band of Landsat 5 can be obtained from the handbooks of the related mission. θ_s and d values can be attained from the metadata file.

For Landsat 8 OLI/TIRS data, reflectance conversion can be applied to DN values directly as in Eq. (4) (Zanter, 2019):

$$\rho_{\lambda} = \frac{M_{\rho}.Q_{CAL} + A_{\rho}}{\sin\theta_{SE}} \qquad (4)$$

where, M_{ρ} is the band-specific multiplicative rescaling factor from the metadata, A_{ρ} is the band-specific additive rescaling factor from the metadata, Q_{CAL} is the quantized and calibrated standard product pixel values (DN) and θ_{SE} is the local sun elevation angle from the metadata file.

Eq. (5) is used to convert the spectral radiance to at-sensor brightness temperature (Wukelic et al., 1989).

$$T_b = \frac{K_2}{\ln(\frac{K_1}{L_{\lambda}} + 1)} \qquad (5)$$

where, T_b is the brightness temperature in Kelvin (K), L_{λ} is the spectral radiance in Wm^{-2}sr^{-1}mm^{-1}; K_2 and K_1 are calibration constants. For Landsat 8 data, K_1 is 774.89, K_2 is 1321.08 (Wm^{-2}sr^{-1}mm^{-1}). For Landsat 7 data, K_1 = 666.09, K_2 = 1282.71 (Wm^{-2}sr^{-1}mm^{-1}). For Landsat 5 data, K_1 is 607.76, K_2 is 1260.56 (Wm^{-2}sr^{-1}mm^{-1}).

The land surface emissivity ε, is estimated using the NDVI Thresholds Method (Sobrino et al., 2004). The fractional vegetation F_v, of each pixel, is determined from the NDVI using the following equation (Carlson & Ripley, 1997):

$$F_v = \left(\frac{NDVI - NDVI_{min}}{NDVI_{max} - NDVI_{min}} \right)^2 \qquad (6)$$

where, $NDVI_{min}$ is the minimum NDVI value (0.2) for bare soil pixel and $NDVI_{max}$ is the maximum NDVI value (0.5) for healthy vegetation pixel.

$d\varepsilon$ is the effect of the geometrical distribution of the natural surfaces and internal reflections. For mixed and elevated land surfaces, the value of $d\varepsilon$ may be 2% (Sobrino et al., 2004).

$$d\varepsilon = (1-\varepsilon_s)(1-F_v)F\varepsilon_v \qquad (7)$$

where, ε_v is vegetation emissivity, ε_s is soil emissivity, F_v is fractional vegetation, F is a shape factor whose mean is 0.55 (Sobrino et al., 2004).

$$\varepsilon = \varepsilon_v F_v + \varepsilon_s(1-F_v) + d\varepsilon \qquad (8)$$

where, ε is the land surface emissivity that is determined by the following equation (Sobrino et al., 2004):

$$\varepsilon = 0.004 * F_v + 0.986 \qquad (9)$$

Water vapour content is estimated by the following equation (Li, 2006; Yang & Qiu, 1996):

$$w = 0.0981 * \left[10 * 0.6108 * \exp\left(\frac{17.27 * (T_0 - 273.15)}{237.3 + (T_0 - 273.15)} \right) * RH \right] + 0.1697 \qquad (10)$$

where, w is the water vapour content (g/cm²), T_0 is the near-surface air temperature in Kelvin (K), RH is the relative humidity (%). These parameters of the atmospheric profile are obtained from the Meteorological Centre, Raipur (http://www.imdraipur.gov.in). Atmospheric transmittance is determined for Raipur City using the following equation (Qin et al., 2001; Sun et al., 2010):

$$\tau = 1.031412 - 0.11536w \qquad (11)$$

where, τ is the total atmospheric transmittance, ε is the land surface emissivity.

Raipur City is located in the tropical region. Thus, the following equations are applied to compute the effective mean atmospheric transmittance of Raipur (Qin et al., 2001; Sun et al., 2010):

$$T_a = 17.9769 + 0.91715T_0 \qquad (12)$$

LST is retrieved from Landsat 5 TM, Landsat 7 ETM+, and Landsat 8 OLI/TIRS satellite data by using the following equations (Qin et al., 2001):

$$T_s = \frac{\left[a(1-C-D)+\left(b(1-C-D)+C+D\right)T_b - DT_a\right]}{C} \qquad (13)$$

$$C = \varepsilon\tau \qquad (14)$$

$$D = (1-\tau)\left[1+(1-\varepsilon)\tau\right] \qquad (15)$$

where, ε is the land surface emissivity, τ is the total atmospheric transmittance, T_b is the at-sensor brightness temperature, T_a is the mean atmospheric temperature, T_0 is the near-surface air temperature, T_s is the land surface temperature, $a = -67.355351$, $b = 0.458606$.

Figure 2 shows the flowchart of methodology of the present study which clearly presents the steps of the LST retrieval process.

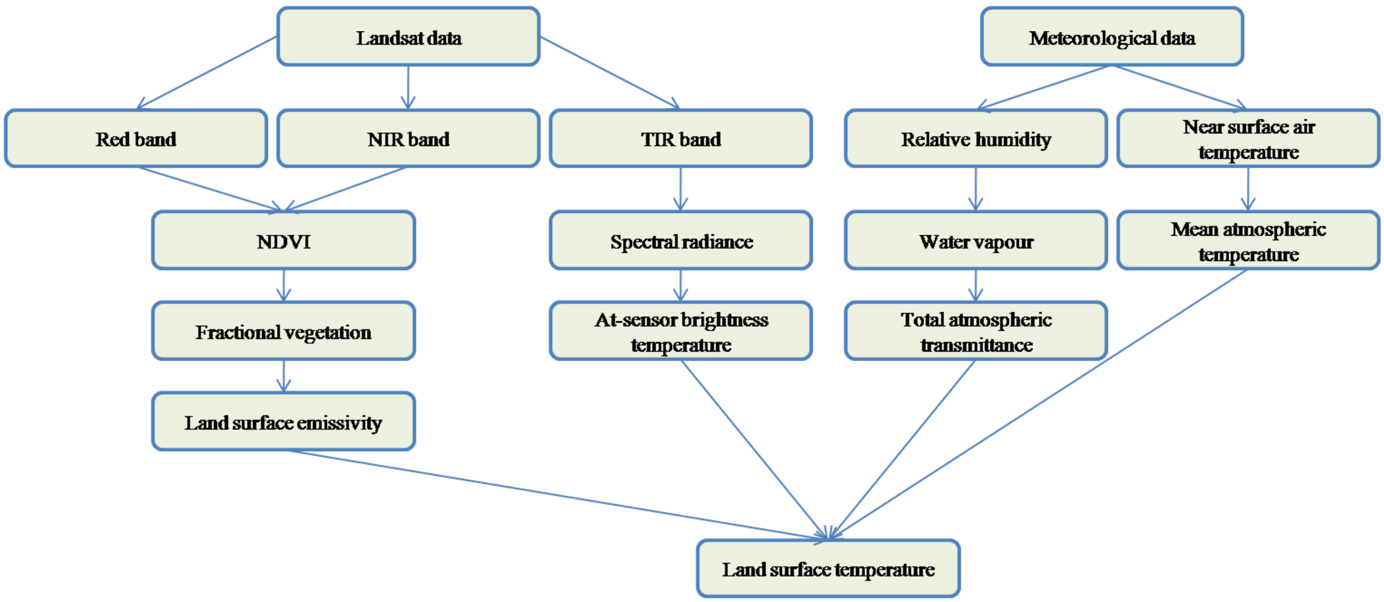

Figure 2 – Flowchart showing the methodology of the present study. Source: Author (2021).

Determination of NDVI

Here, NDVI was selected as a normalized difference spectral index in the research work (Tucker, 1979). NDVI is determined by the red and NIR bands. For TM and ETM+ data, band 3 is used as a red band and band 4 is used as a NIR band, respectively. For OLI/TIRS data, band 4 and band 5 are used as red and NIR bands, respectively (Table 4). The value of NDVI ranges between −1 and +1. Generally, the negative value of NDVI indicates the water surfaces. Positive NDVI shows vegetation surface. The increasing positive value of NDVI indicates the increase of greenness in plants.

Table 4 – Description of normalized difference vegetation index (NDVI)

Acronym	Description	Formulation	References
NDVI	Normalized difference vegetation index	$\frac{NIR - \mathrm{Re}\,d}{NIR + \mathrm{Re}\,d}$	Tucker 1979

Source: Author (2020).

Results and discussion

Monthly variation in LST distribution

Table 5 shows a clear observation of monthly change in the mean LST values. In this table, the mean LST of each image is shown. The mean LST of every month was also determined. In this way, the mean LST values for ten months (no cloud-free data was available for July and August) were presented.

It is seen from Table 5 that the mean LST of the city was above 32°C mean LST for all the months from March-May of 1992, 2001-02, 2004-05, 2008-11, 2013, 2016-17, and 2019. June and September of 2005, 2006, and 2009 have more mean LST values than the earlier and later years. The scenario was completely different from October to February, where that the mean LST of the city was below 28°C LST. April (38.79°C mean LST), May (36.65°C mean LST), June (34.56°C mean LST), and March (32.11°C mean LST) - these four months have an average value of > 35°C mean LST throughout the entire period of study. February (27.88°C mean LST), October (27.23°C mean LST), September (27.18°C mean LST), and November (25.83°C mean LST) - these four months have an average value of 25-28°C mean LST throughout the entire time. Only December (23.76°C mean LST) and January (23.01°C mean LST) months have an average value of < 24°C mean LST for the period. The average value of the highest and the lowest mean LST from 1988 to 2019 is observed in April and January, respectively. The northwest and southeast parts of the study area exhibit high LST. These parts also have a low percentage of urban vegetation and a high percentage of built-up areas and bare land. It shows that the proportion of vegetation reduced significantly with time.

Figure 3 shows the line graph of LST in different months from 1988 o 2019. October, November, and December present an almost similar pattern of LST distribution. January and February show an almost similar trend in their LST graph. A similarity also has been seen in the mean LST graph of March, April, and May. The LST graph of June shows a negative trend, while September shows a positive trend.

Table 5 – Monthly distribution of mean LST (°C) for the entire Raipur City from 1988 to 2019

January	LST (°C)	February	LST (°C)	March	LST (°C)	April	LST (°C)	May	LST (°C)
1988-Jan-21	24.52	1989-Feb-24	28.31	1989-Mar-12	28.14	1990-Apr-16	40.87	1991-May-21	36.63
1990-Jan-10	24.42	1990-Feb-11	25.26	1990-Mar-15	30.96	1992-Apr-21	41.19	2002-May-11	40.92
1992-Jan-16	21.33	1991-Feb-14	23.98	1991-Mar-18	29.50	1995-Apr-14	34.63	2004-May-24	40.74
1993-Jan-18	23.41	1992-Feb-17	25.30	1992-Mar-20	32.84	2001-Apr-22	41.34	2005-May-11	38.72
1996-Jan-27	22.08	1993-Feb-19	28.42	2003-Mar-11	29.49	2002-Apr-25	38.85	2006-May-14	28.43
2005-Jan-19	22.08	2002-Feb-20	30.39	2004-Mar-21	36.48	2003-Apr-12	31.28	2007-May-17	36.20
2007-Jan-25	26.37	2004-Feb-18	26.64	2007-Mar-14	27.57	2004-Apr-22	36.80	2008-May-19	38.36
2009-Jan-14	17.15	2006-Feb-23	32.95	2009-Mar-19	33.79	2009-Apr-20	39.74	2009-May-22	33.20
2011-Jan-20	23.03	2009-Feb-15	31.01	2014-Mar-17	31.68	2010-Apr-23	40.63	2010-May-25	36.11
2015-Jan-15	23.49	2010-Feb-18	22.67	2015-Mar-20	32.83	2016-Apr-23	42.97	2011-May-12	39.80
2018-Jan-23	25.26	2015-Feb-16	29.75	2016-Mar-22	37.00	2017-Apr-10	38.37	2013-May-17	40.28
		2016-Feb-19	24.60	2017-Mar-25	37.06			2014-May-20	34.91
		2017-Feb-21	32.45	2018-Mar-12	30.09			2015-May-23	36.42
		2018-Feb-24	31.05					2016-May-25	37.22
		2019-Feb-11	25.37					2017-May-12	33.33
		1989-Feb-24	28.31					2018-May-15	31.42
								2019-May-18	40.21
Mean	*23.01*	*Mean*	*27.88*	*Mean*	*32.11*	*Mean*	*38.79*	*Mean*	*36.64*
June	**LST (°C)**	**September**	**LST (°C)**	**October**	**LST (°C)**	**November**	**LST (°C)**	**December**	**LST (°C)**
2005-Jun-12	38.66	1996-Sep-23	24.09	1988-Oct-19	28.86	1988-Nov-20	24.27	1988-Dec-22	23.96
2006-Jun-15	35.43	2001-Sep-21	26.13	1991-Oct-12	24.98	1989-Nov-23	25.16	1992-Dec-17	22.34
2009-Jun-23	33.05	2002-Sep-16	28.81	1992-Oct-14	24.61	1991-Nov-13	23.64	1994-Dec-23	18.55
2018-Jun-16	31.08	2014-Sep-25	29.67	1996-Oct-25	22.56	1993-Nov-18	24.47	1995-Dec-10	21.49
				2001-Oct-15	30.12	1996-Nov-10	23.15	2000-Dec-15	26.81
				2001-Oct-23	26.85	1999-Nov-11	29.16	2002-Dec-21	27.09
				2004-Oct-15	27.56	2004-Nov-16	28.45	2004-Dec-18	25.76
				2006-Oct-21	26.30	2005-Nov-19	26.72	2006-Dec-24	23.35
				2009-Oct-13	27.10	2006-Nov-22	26.40	2008-Dec-13	25.71
				2011-Oct-19	28.30	2008-Nov-11	27.38	2009-Dec-16	23.59
				2015-Oct-14	27.61	2013-Nov-25	26.09	2010-Dec-19	22.31
				2016-Oct-16	30.02	2014-Nov-12	23.47	2013-Dec-11	24.62
				2018-Oct-22	29.01	2016-Nov-17	27.18	2016-Dec-19	24.60
						2017-Nov-20	26.28	2017-Dec-22	24.02
						2019-Nov-10	25.60	2018-Dec-25	21.17
								2019-Dec-12	24.74
Mean	*34.56*	*Mean*	*27.18*	*Mean*	*27.22*	*Mean*	*25.83*	*Mean*	*23.76*

Source: Author (2021).

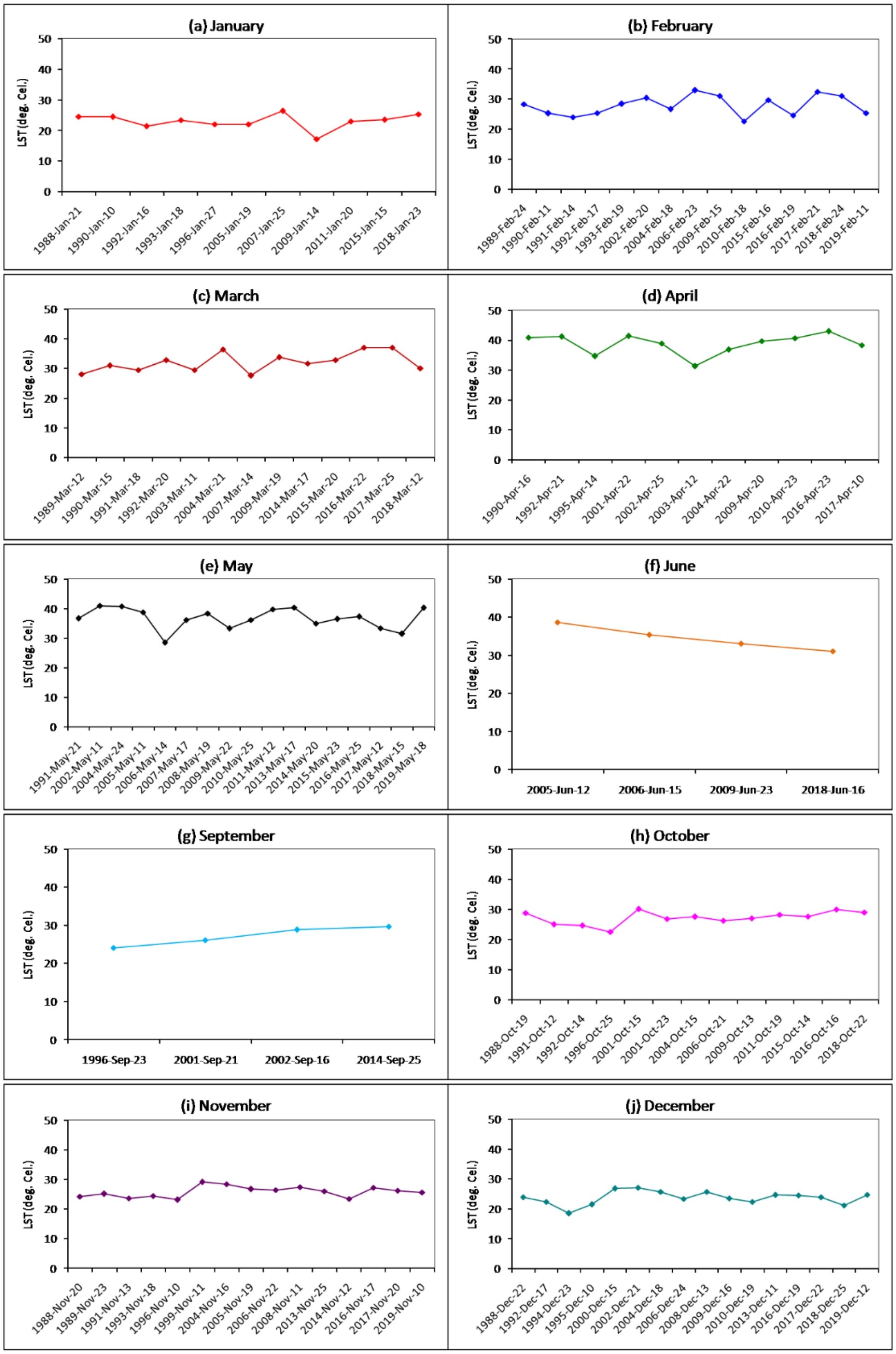

Figure 3 – Line graphs for monthly **v**ariation of LST (ºC) from1988 to 2019: (a) January (b) February (c) March (d) April (e) May (f) June (g) September (h) October (i) November (j) December. Source: Author (2021).

Monthly variation on LST-NDVI relationship

Table 6 – Monthly variation of LST-NDVI correlation coefficient(1988-2019) (significant at 0.05 level)

January	Correlation coefficient	February	Correlation coefficient	March	Correlation coefficient	April	Correlation coefficient	May	Correlation coefficient
1988-Jan-21	-0.31	1989-Feb-24	-0.39	1989-Mar-12	-0.43	1990-Apr-16	-0.52	1991-May-21	-0.43
1990-Jan-10	-0.36	1990-Feb-11	-0.38	1990-Mar-15	-0.43	1992-Apr-21	-0.53	2002-May-11	-0.56
1992-Jan-16	-0.35	1991-Feb-14	-0.12	1991-Mar-18	-0.40	1995-Apr-14	-0.38	2004-May-24	-0.46
1993-Jan-18	-0.38	1992-Feb-17	-0.29	1992-Mar-20	-0.40	2001-Apr-22	-0.65	2005-May-11	-0.54
1996-Jan-27	-0.30	1993-Feb-19	-0.37	2003-Mar-11	-0.41	2002-Apr-25	-0.57	2006-May-14	-0.46
2005-Jan-19	-0.21	2002-Feb-20	-0.44	2004-Mar-21	-0.49	2003-Apr-12	-0.39	2007-May-17	-0.33
2007-Jan-25	-0.21	2004-Feb-18	-0.30	2007-Mar-14	-0.38	2004-Apr-22	-0.51	2008-May-19	-0.48
2009-Jan-14	-0.25	2006-Feb-23	-0.31	2009-Mar-19	-0.54	2009-Apr-20	-0.56	2009-May-22	-0.44
2011-Jan-20	-0.18	2009-Feb-15	-0.36	2014-Mar-17	-0.42	2010-Apr-23	-0.52	2010-May-25	-0.47
2015-Jan-15	-0.27	2010-Feb-18	-0.24	2015-Mar-20	-0.36	2016-Apr-23	-0.46	2011-May-12	-0.56
2018-Jan-23	-0.15	2015-Feb-16	-0.16	2016-Mar-22	-0.40	2017-Apr-10	-0.51	2013-May-17	-0.43
		2016-Feb-19	-0.21	2017-Mar-25	-0.43			2014-May-20	-0.41
		2017-Feb-21	-0.30	2018-Mar-12	-0.37			2015-May-23	-0.34
		2018-Feb-24	-0.28					2016-May-25	-0.38
		2019-Feb-11	-0.21					2017-May-12	-0.29
		1989-Feb-24	-0.39					2018-May-15	-0.45
								2019-May-18	-0.43
Mean	*-0.24*	*Mean*	*-0.29*	*Mean*	*-0.40*	*Mean*	*-0.51*	*Mean*	*-0.44*
June	**Correlation coefficient**	**September**	**Correlation coefficient**	**October**	**Correlation coefficient**	**November**	**Correlation coefficient**	**December**	**Correlation coefficient**
2005-Jun-12	-0.51	1996-Sep-23	-0.54	1988-Oct-19	-0.69	1988-Nov-20	-0.41	1988-Dec-22	-0.20
2006-Jun-15	-0.46	2001-Sep-21	-0.58	1991-Oct-12	-0.63	1989-Nov-23	-0.29	1992-Dec-17	-0.15
2009-Jun-23	-0.42	2002-Sep-16	-0.56	1992-Oct-14	-0.68	1991-Nov-13	-0.38	1994-Dec-23	-0.24
2018-Jun-16	-0.46	2014-Sep-25	-0.53	1996-Oct-25	-0.64	1993-Nov-18	-0.19	1995-Dec-10	-0.09
				2001-Oct-15	-0.66	1996-Nov-10	-0.40	2000-Dec-15	-0.18
				2001-Oct-23	-0.58	1999-Nov-11	-0.48	2002-Dec-21	-0.29
				2004-Oct-15	-0.63	2004-Nov-16	-0.35	2004-Dec-18	-0.10
				2006-Oct-21	-0.51	2005-Nov-19	-0.31	2006-Dec-24	-0.23
				2009-Oct-13	-0.64	2006-Nov-22	-0.23	2008-Dec-13	-0.12
				2011-Oct-19	-0.63	2008-Nov-11	-0.41	2009-Dec-16	-0.20
				2015-Oct-14	-0.61	2013-Nov-25	-0.44	2010-Dec-19	-0.24
				2016-Oct-16	-0.53	2014-Nov-12	-0.52	2013-Dec-11	-0.19
				2018-Oct-22	-0.63	2016-Nov-17	-0.44	2016-Dec-19	-0.21
						2017-Nov-20	-0.45	2017-Dec-22	-0.30
						2019-Nov-10	-0.59	2018-Dec-25	-0.22
								2019-Dec-12	-0.40
Mean	*-0.47*	*Mean*	*-0.55*	*Mean*	*-0.62*	*Mean*	*-0.39*	*Mean*	*-0.21*

Source: Author (2021).

Table 6 represents a monthly variation of Pearson's linear correlation method between LST and NDVI significant at 0.05 level. On average, October (-0.62), September (-0.55), and April (-0.51) months build a strong negative correlation. June (-0.47), May (-0.44), March (-0.44), and November (-0.39) months have a moderate negative correlation. A weak negative correlation was found in February (-0.29), January (-0.24), and December (-0.21) months. The main reason behind the strong to moderate LST-NDVI correlation in March-November is the presence of high intensity of moisture and chlorophyll content in green vegetation. Dry months reduce the strength of regression, while wet months enhance the strength of the LST-NDVI regression. Hence, the climatic condition and surface material influence the LST-NDVI correlation analysis.

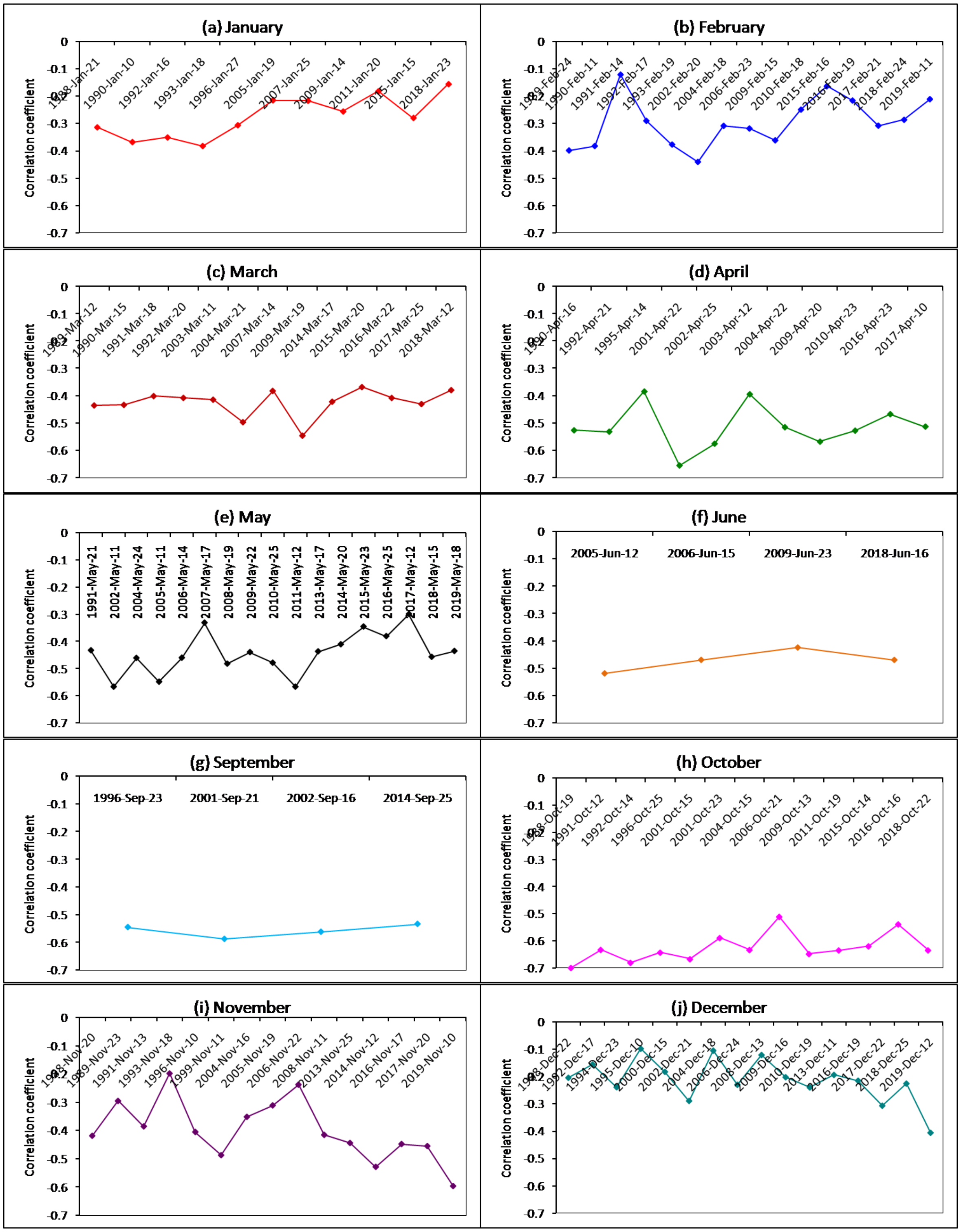

Figure 4 – Line graphs for monthly **v**ariation of LST-NDVI relationship (1988-2019): (a) January (b) February (c) March (d) April (e) May (f) June (g) September (h) October (i) November (j) December. Source: Author (2021).

Figure 4 shows the line graphs for monthly variation of LST-NDVI relationships. June and September months show a smooth convex and concave trend, respectively due to wet weather. The line graphs of October, November, and December show more fluctuation due to more differences in atmospheric components. The line graphs of January and March look almost similar. February, April, and May present similar trends of LST.

Liang et al. (2012) presented similar types of negative NDVI-LST correlation in Guilin City, China. In high latitudes, positive LST-NDVI relationships have been observed as the presence of vegetation increases the value of LST in high latitudes where the winter season is severe (Karnieli et al., 2006). Yue et al. (2007) showed that the LST-NDVI relationship in Shanghai City, China was negative and was different in different LULC types like the relationship was strong negative on vegetation. Sun and Kafatos (2007) stated that the LST-NDVI correlation was positive in the winter season while it was negative in the summer season as the winter season produces the lowest LST on the rock surface and dry soil and vice-versa in the summer season. This relationship was also negative in Mashhad, Iran as it is a dry tropical city (Gorgani et al., 2013). The relationship was strongly negative in Berlin City for any season (Marzban et al., 2018). This correlation tends to be more negative with the increase of surface moisture as in the wet season more green and healthy vegetation is produced (Moran et al., 1994; Lambin & Ehrlich, 1996; Prehodko & Goward, 1997; Sandholt et al., 2002). The present study also found a negative LST-NDVI correlation for all the months as it is a humid tropical city. The value of the correlation coefficient is inversely related to the surface moisture content, i.e., the negativity of the relationship increases with the increase of surface moisture content.

Conclusions

The present study estimates the monthly variation of LST distribution in Raipur City, India using one hundred and eighteen Landsat datasets from 1988 to 2019. April, May, June, and March present higher LST values than the rest of the months. The present study also assesses the monthly correlation of LST and NDVI in Raipur City. In general, the results show that LST is inversely related to NDVI, irrespective of any month. From March to November, the correlation is strong to moderate negative, whereas it is found weak negative in the winter season (December to February). The presence of healthy green plants and high moisture content in the air is the main responsible factors for strong negativity. The study is useful for the environmentalists and urban planners for future ecological planning from several points of view. Special attention may be taken in March, April, May, and June to increase the negativity of the relationship by plantation. Simultaneously, more trees can be planted in December, January, and February for generating pleasant weather. Moreover, some commercial activities may be decreased in the winter months as at that time the city remains dry and more polluted. Special emphasis should be taken on the transport and industrial sectors as these sectors are mainly responsible for generating high LST. Mass transport system must be encouraged instead of the private transport system. The area under the park, urban vegetation, water bodies, and wetland must be increased at any cost as these changes can bring ecological comfort to the city. The unused fallow lands should be converted into vegetation and water area. It will be beneficial to the residents if any public and private initiatives have to be taken on seasonal plantation programmes along the roadways and barren lands.

References

Alexander, C. (2020). Normalised difference spectral indices and urban land cover as indicators of land surface temperature (LST). *Int J Appl Earth Obs Geoinf,* 86, 102013. https://doi.org/10.1016/j.jag.2019.102013.

Carlson, T. N., & Ripley, D. A. (1997). On the Relation between NDVI, Fractional Vegetation Cover, and Leaf Area Index. *Remote Sens Environ*, 62(3), 241-252. https://doi.org/10.1016/S0034-4257(97)00104-1.

Chen, XL, Zhao, HM, Li, PX, & Yi, ZY. (2006). Remote sensing image-based analysis of the relationship between urban heat island and land use/cover changes. *Remote Sens Environ,* 104(2), 133–146. https://doi.org/10.1016/j.rse.2005.11.016

Cui, L., Wang, L., Qu, S., Singh, R. P., Lai, Z., & Yao, R. (2019). Spatiotemporal extremes of temperature and precipitation during 1960–2015 in the Yangtze River Basin (China) and impacts on vegetation dynamics. *Theor Appl Climatol,* 136(1-2), 675-692. https://doi.org/10.1007/s00704-018-2519-0.

Cui, L., Wang, L., Qu, S., Singh, R. P., Lai, Z., Jiang, L., & Yao, R. (2019). Association analysis between spatiotemporal variation of vegetation greenness and precipitation/temperature in the Yangtze River Basin (China). *Environ Sci Pollut Res,* 25(22), 21867–21878. https://doi.org/10.1007/s11356-018-2340-4.

Fatemi, M., & Narangifard, M. (2019). Monitoring LULC changes and its impact on the LST and NDVI in District 1 of Shiraz City. *Arab J Geosci,* 12, 127. https://doi.org/10.1007/s12517-019-4259-6.

Ferrelli, F., Huamantinco, M. A., Delgado, D. A., & Piccolo, M. C. (2018). Spatial and temporal analysis of the LST-NDVI relationship for the study of land cover changes and their contribution to urban planning in Monte Hermoso, Argentina. *Doc Anal Geogr*, 64(1), 25-47. https://doi.org/10.5565/rev/dag.355.

Ghobadi, Y., Pradhan, B., Shafri, H. Z. M., & Kabiri, K. (2014). Assessment of spatial relationship between land surface temperature and land use/cover retrieval from multi-temporal remote sensing data in South Karkheh Sub-basin, Iran. *Arab J Geosci,* 8(1), 525–537. https://doi.org/10.1007/s12517-013-1244-3.

Gorgani, S. A., Panahi, M., & Rezaie, F. (2013). The relationship between NDVI and LST in the Urban area of Mashhad, Iran. In *International Conference on Civil Engineering Architecture and Urban Sustainable Development*. November, Tabriz, Iran.

Govil, H., Guha, S., Dey, A., & Gill, N. (2019). Seasonal evaluation of downscaled land surface temperature: A case study in a humid tropical city. *Heliyon,* 5(6), e01923. https://doi.org/10.1016/j.heliyon.2019.e01923.

Govil, H., Guha, S., Diwan, P., Gill, N., & Dey, A. (2020). Analyzing Linear Relationships of LST with NDVI and MNDISI Using Various Resolution Levels of Landsat 8 OLI/TIRS Data. In Sharma N., Chakrabarti A., Balas V. (Eds.), *Data Management, Analytics and Innovation. Advances in Intelligent Systems and Computing* (Vol. 1042, p. 171-184). Singapore: Springer. https://doi.org/10.1007/978-981-32-9949-8_13

Goward, S. N., Xue, Y. K., & Czajkowski, K. P. (2002). Evaluating Land Surface Moisture Conditions from the Remotely Sensed Temperature/Vegetation Index Measurements: An Exploration with the Simplified Simple Biosphere Model. *Remote Sens Environ,*79, 225-242. https://doi:10.1016/S0034-4257(01)00275-9.

Guha, S. (2016). Capability of NDVI technique in detecting mangrove vegetation. *Int J Adv Biol Res,* 6(2), 253-258.

Guha, S. (2021). Dynamic seasonal analysis on LST-NDVI relationship and ecological health of Raipur City, India. *Ecosyst Health Sustain.* 7(1): 1927852. https://doi.org/10.1080/20964129.2021.1927852.

Guha, S., & Govil, H. (2019). Evaluation of ASTER TIR data-based lithological indices in Malanjkhand Copper Mines of Madhya Pradesh, India. *Appl Earth Sci,* 129(1), 3-8. https://doi.org/10.1080/25726838.2019.1684018.

Guha, S., & Govil, H. (2020). Seasonal impact on the relationship between land surface temperature and normalized difference vegetation index in an urban landscape. *Geocarto Int*. https://doi.org/10.1080/10106049.2020.1815867.

Guha, S., & Govil, H. (2021a). Annual assessment on the relationship between land surface temperature and six remote sensing indices using Landsat data from 1988 to 2019. *Geocarto Int*. https://doi.org/10.1080/10106049.2021.1886339.

Guha, S., & Govil, H. (2021b). COVID-19 lockdown effect on land surface temperature and normalized difference vegetation index. *Geomat Nat Haz Risk,* 12(1): 1082-1100. https://doi.org/10.1080/19475705.2021.1914197.

Guha, S., & Govil, H. (2021c). An assessment on the relationship between land surface temperature and normalized difference vegetation index. *Environ Dev Sustain,*23(2): 1944-1963. https://doi.org/10.1007/s10668-020-00657-6.

Guha, S., Govil, H., & Besoya, M. (2020). An investigation on seasonal variability between LST and NDWI in an urban environment using Landsat satellite data. *Geomat Nat Haz Risk*, 11(1), 1319-1345. https://doi.org/10.1080/19475705.2020.1789762.

Guha, S., Govil, H., & Diwan, P. (2019). Analytical study of seasonal variability in land surface temperature with normalized difference vegetation index, normalized difference water index, normalized difference built-up index, and normalized multiband drought index. *J Appl Remote Sens,* 13(2), 024518. https://doi.org/1010.1117/1.JRS.13.024518.

Guha, S., Govil, H., & Diwan, P. (2020). Monitoring LST-NDVI Relationship Using Premonsoon Landsat Datasets. *AdvMeteorol*, 2020, 4539684. https://doi.org/10.1155/2020/4539684.

Guha, S., Govil, H., & Mukherjee, S. (2017). Dynamic analysis and ecological evaluation of urban heat islands in Raipur city, India. *J Appl Remote Sens*, 11(3), 036020. https://doi.org/10.1117/1.JRS.11.036020.

Guha, S., Govil, H., Dey, A., & Gill, N. (2018). Analytical study of land surface temperature with NDVI and NDBI using Landsat 8 OLI/TIRS data in Florence and Naples city, Italy. *Eur J Remote Sens*, 51(1), 667-678. https://doi:10.1080/22797254.2018.1474494.

Guha, S., Govil, H., Dey, A., & Gill, N. (2020). A case study on the relationship between land surface temperature and land surface indices in Raipur City, India. *Geogr Tidsskr,*120(1), 35-50. https://doi.org/10.1080/00167223.2020.1752272.

Guha, S., Govil, H., Gill, N., & Dey, A. (2020a). A long-term seasonal analysis on the relationship between LST and NDBI using Landsat data. *Quatern Int*. 575-576: 249-258. https://doi.org/10.1016/j.quaint.2020.06.041

Guha, S., Govil, H., Gill, N., & Dey, A. (2020b). Analysing the Capability of NCI Technique in Change Detection Using High-and Medium-Resolution Multispectral Data. In S. Sahdev, R. B. Singh, & M. Kumar (Eds.), *Geoecology of Landscape Dynamics* (p. 133-147). Springer, Singapore. https://doi.org/10.1007/978-981-15-2097-6_10.

Guha, S., Govil, H., Gill, N., & Dey, A. (2020c). Analytical study on the relationship between land surface temperature and land use/land cover indices. *Ann GIS*, 26(2), 201-216. https://doi.org/10.1080/19475683.2020.1754291.

Gui, X., Wang, L., Yao, R., Yu, D., & Li, C. (2019). Investigating the urbanization process and its impact on vegetation change and urban heat island in Wuhan, China. *Environ Sci Pollut Res*, 26(30), 30808-30825. https://doi.org/10.1007/s11356-019-06273-w.

Gutman, G., & Ignatov, A. (1998). The Derivation of the Green Vegetation Fraction from NOAA/ AVHRR Data for Use in Numerical Weather Prediction Models. *Int J Remote Sens,* 19(8), 1533-1543. https://doi:10.1080/014311698215333.

Hao, X., Li, W., & Deng, H. (2016). The oasis effect and summer temperature rise in arid regions-case study in Tarim Basin. *Sci Rep,* 6, 35418. https://doi.org/10.1038/srep35418.

Hou, G. L., Zhang, H. Y., Wang, Y. Q., Qiao, Z. H., & Zhang, Z. X. (2010). Retrieval and Spatial Distribution of Land Surface Temperature in the Middle Part of Jilin Province Based on MODIS Data. *SciGeogr Sin,* 30, 421–427.

Jamei, Y., Rajagopalan, P., & Sun, Q. C. (2019). Spatial structure of surface urban heat island and its relationship with vegetation and built-up areas in Melbourne, Australia. *Sci Total Environ,* 659, 1335-1351. https://doi.org/10.1016/j.scitotenv.2018.12.308.

Karnieli, A., Bayasgalan, M., Bayarjargal, Y., Agam, N., Khudulmur, S., & Tucker, C. J. (2006). Comments on the use of the Vegetation Health Index over Mongolia. *Int J Remote Sens*, 27(10), 2017-2024. https://doi:10.1080/01431160500121727.

Kikon, N., Singh, P., Singh, S. K., & Vyas, A. (2016). Assessment of urban heat islands (UHI) of Noida City, India using multi-temporal satellite data. *Sustain Cities Soc*, 22, 19-28. https://doi.org/10.1016/j.scs.2016.01.005.

Kumar, D., & Shekhar, S. (2015). Statisticalanalysisofland surface temperature–vegetation indexes relationship through thermal remote sensing. *Ecotox Environ Safe*, 121, 39-44. https://doi.org/10.1016/j.ecoenv.2015.07.004.

Lambin, E. F., & Ehrlich, D. (1996). The Surface Tenperature-Vegetation Index Space for Land Use and Land Cover Change analysis. *Int J Remote Sens,* 17, 463-487. https://doi.org/10.1080/01431169608949021.

Li, J. (2006). Estimating land surface temperature *from Landsat-5 TM. Remote Sens Technol Appl,*21, 322-326.

Li, W. F., Cao, Q. W., Kun, L., & Wu, J. S. (2017). Linking potential heat source and sink to urban heat island: Heterogeneous effects of landscape pattern on land surface temperature. *Sci Total Environ,* 586, 457–465. https://doi.org/10.1016/j.scitotenv.2017.01.191.

Liang, B. P., Li, Y., & Chen, K. Z. (2012). A Researchon Land Features and Correlation between NDVI and Land Surface Temperature in Guilin City. *Remote Sens Tech Appl*, 27, 429–435.

Marzban, F., Sodoudi, S., & Preusker, R. (2018). The influence of land-cover type on the relationship between LST-NDVI and LST-T_{air}. *Int J Remote Sens*, 39(5), 1377-1398. https://doi.org/10.1080/01431161.2017.1462386.

Mathew, A., Khandelwal, S., & Kaul, N. (2017). Investigating spatial and seasonal variations of urban heat island effect over Jaipur city and its relationship with vegetation, urbanization and elevation parameters. *Sustain Cities Soc*, 35, 157-177. https://doi.org/10.1016/j.scs.2017.07.013.

Mathew, A., Khandelwal, S., & Kaul, N. (2018). Spatio-temporal variations of surface temperatures of Ahmedabad city and its relationship with vegetation and urbanization parameters as indicators of surface temperatures. *Remote Sens Appl Soc Environ*, 11, 119-139. https://doi.org/10.1016/j.rsase.2018.05.003.

Mondal, A., Guha, S., Mishra, P. K., & Kundu, S. (2011). Land use/Land cover changes in Hugli Estuary using Fuzzy CMean algorithm. Int J Geomat Geosci, 2(2), 613-626.

Moran, M. S., Clarke, T. R., Inouie, Y., & Vidal, A. (1994). Estimating Crop Water-Deficit using the Relation between Surface Air-Temperature and Spectral Vegetation Index. *Remote Sens Environ*, 49, 246-263. https://doi.org/10.1016/0034-4257(94)90020-5.

Prehodko, L., & Goward, S. N. (1997). Estimation of Air Temperature from Remotely Sensed Surface Observations. *Remote Sens Environ, 60, 335–346. htt*ps://doi:10.1016/S0034-4257 (96)00216-7.

Qin, Z., Karnieli, A., & Barliner, P. (2001). A Mono-WindowAlgorithm for Retrieving Land Surface Temperature from Landsat TM Data and Its Application to the Israel-Egypt Border Region. *Int J Remote Sens*, 22(18), 3719-3746. https://doi:10.1080/01431160010006971.

Qu, S., Wang, L., Lin, A., Yu, D, Yuan, M., & Li, C. (2020). Distinguishing the impacts of climate change and anthropogenic factors on vegetation dynamics in the Yangtze River Basin, China. *Ecol Indic*, 108, 105724. https://doi.org/10.1016/j.ecolind.2019.105724.

Qu, S., Wang, L., Lin, A., Zhu, H., & Yuan, M. (2018). What drives thevegetation restoration in Yangtze River basin, China: Climate change or anthropogenic factors? *Ecol Indic,* 90, 438–450. https://doi.org/10.1016/j.ecolind.2018.03.029.

Sandholt, I., Rasmussen, K., & Andersen, J. (2002). A simple interpretation of the Surface Temperature/Vegetation Index Space for Assessment of Surface Moisture Status. Remote Sens Environ, 79, 213-224. https://doi.org/10.1016/s0034-4257(01)00274-7.

Sannigrahi, S., Bhatt, S., Rahmat, S., Uniyal, B., Banerjee, S., Chakraborti, S., Jha, S., Lahiri, S., Santra, K., & Bhatt, A. (2018). Analyzing the role of biophysical compositions in minimizing urban land surface temperature and urban heating*Urban Climate*, 24, 803-819. https://doi.org/10.1016/j.uclim.2017.10.002.

Sekertekin, A., & Bonafoni, S. (2020). Land surface temperature retrieval from landsat 5, 7, and 8 over rural areas: assessment of different retrieval algorithms and emissivity models and toolbox implementation. *Remote Sens*, 12(2), 294.

Shigeto, K. (1994). Relation between vegetation, surface temperature, and surface composition in the Tokyo region during winter. *Remote Sens Environ,* 50(1), 52–60. https://doi.org/10.1016/0034-4257(94)90094-9

Singh, P., Kikon, N., & Verma, P. (2017). Impact of land use change and urbanization on urban heat island in Lucknow city, Central India. A remote sensing based estimate. *Sustain Cities Soc*, 32, 100-114. https://doi.org/10.1016/j.scs.2017.02.018.

Sobrino, J. A., Jimenez-Munoz, J. C., & Paolini, L. (2004). Land surface temperature retrieval from Landsat TM5. *Remote Sens Environ,*90(4), 434–440. https://doi.org/10.1016/j.rse.2004.02.003.

Sun, D., & Kafatos, M. (2007). Note on the NDVI-LST Relationship and the Use of Temperature-Related Drought Indices over North America. *Geophys Res Lett*, 34(24), L24406. http://doi.org/10.1029/2007GL031485.

Sun, Q., Tan, J., & Xu, Y. (2010). An ERDAS image processing method for retrieving LST and describing urban heat evolution: A case study in the Pearl River Delta Region in South China. *Environ Earth Sci,* 59, 1047-1055. https://doi.org/10.1007/s12665-009-0096-3.

Tomlinson, C. J., Chapman, L., Trones, J. E., & Baker, C. (2011). Remote sensingland surface temperature for meteorology and climatology: a review. *Meteorol Appl,* 18, 296–306. https://doi.org/10.1002/met.287.

Tucker, C. J. (1979). Red and photographic infrared linear combinations for monitoring vegetation. *Remote Sens Environ,* 8(2), 127–150.

USGS: Science for a Changing World. *EarthExplorer*. Retrieved from https://www.earthexplorer.usgs.gov

Voogt, J. A., & Oke, T. R. (2003). Thermal Remote Sensing of Urban Climates. *Remote Sens Environ,* 86, 370-384. https://doi.org/10.1016/S0034-4257(03)00079-8.

Wang, J., Qingming, Z., Guo, H., & Jin, Z. (2016). Characterizing the spatial dynamics of land surface temperature–impervious surface fraction relationship. *Int J Appl Earth Obs Geoinf*, 45, Part-A, 55–65. https://doi.org/10.1016/j.jag.2015.11.006.

Wang, L., Lu, Y., & Yao, Y. (2019). Comparison of three algorithms for the retrieval of land surface temperature from Landsat 8 images. *Sensors*, 19(22), 5049.

Wen, L., Peng, W., Yang, H., Wang, H., Dong, L., & Shang, X. (2017). An analysis of land surface temperature (LST) and its influencing factors in summer in western Sichuan Plateau: A case study of Xichang City. *Remote Sens Land Res,* 29(2), 207–214. https://doi.org/10.6046/gtzyyg.2017.02.30.

Wukelic, G. E., Gibbons, D. E., Martucci, L. M., & Foote, H. P. (1989). Radiometric calibration of Landsat Thematic Mapper thermal band. *Remote Sens Environ*, 28, 339–347.

Yang, J., & Qiu, J. (1996). The empirical expressions of the relation between precipitable water and ground water vapor pressure for some areas in China. *Sci Atmos Sinica*, 20, 620-626.

Yao, R., Cao, J., Wang, L., Zhang, W., & Wu, X. (2019). Urbanization effects on vegetation cover in major African cities during 2001-2017. *Int J Appl Earth Obs*, 75, 44-53. https://doi.org/10.1016/j.jag.2018.10.011.

Yao, R., Wang, L., Gui, X., Zheng, Y., Zhang, H., & Huang, X. (2017). Urbanization Effects on Vegetation and Surface Urban Heat Islands in China's Yangtze River Basin. *Remote Sens*, 9(6), 540. https://doi.org/10.3390/rs9060540.

Yao, R., Wang, L., Huang, X., Chen, J., Li, J., &Niu, Z. (2018). Less sensitive of urban surface to climate variability than rural in Northern China. *Sci Total Environ,* 628-629, 650-660. https://doi.org/10.1016/j.scitotenv.2018.02.087.

Yao, R., Wang, L., Huang, X., Chen, X., & Liu, Z. (2019). Increased spatial heterogeneity in vegetation greenness due to vegetation greening in mainland China. *Ecol Indic,* 99, 240-250. https://doi.org/10.1016/j.ecolind.2018.12.039.

Yao, R., Wang, L., Huang, X., Niu, Z., Liu, F., & Wang, Q. (2017). Temporal trends of surface urban heat islands and associated determinants in major Chinese cities. *Sci Total Environ*, 609, 742-754. https://doi.org/10.1016/j.scitotenv.2017.07.217.

Yao, R., Wang, L., Huang, X., Zhang, W., Li, J., & Niu, Z. (2018). Interannual variations in surface urban heat island intensity and associated drivers in China. *J Environ Manage,* 222, 86-94. https://doi.org/10.1016/j.jenvman.2018.05.024.

Yuan, M., Wang, L., Lin, A., Liu, Z., & Qu, S. (2020). Vegetation green up under the influence of daily minimum temperature and urbanization in the Yellow River Basin, China. *Ecol Indic*, 108, 105760. https://doi.org/10.1016/j.ecolind.2019.105760.

Yuan, X., Wang, W., Cui, J., Meng, F., Kurban, A., & De Maeyer, P. (2017). Vegetation changes and land surface feedbacks drive shifts in local temperatures over Central Asia. *Sci Rep*, 7(1), 3287. https://doi.org/10.1038/s41598017034322.

Yue, W., Xu, J., Tan, W., &Xu, L. (2007). The Relationship between Land Surface Temperature and NDVI with Remote Sensing. Application to Shanghai Landsat 7 ETM+ data. *Int J Remote Sens*, 28, 3205–3226. https://doi.org/10.1080/01431160500306906.

Zanter, K. (2019). *Landsat 8 (L8) Data Users Handbook*. EROS, Sioux Falls, SD, USA.

Editor: Fábio Duarte

Received: Sep. 25th, 2020

Approved: Jun. 30th,2021